IEEE Access
Multidisciplinary | Rapid Review | Open Access Journal

Received January 15, 2021, accepted February 3, 2021, date of publication February 11, 2021, date of current version March 5, 2021.

Digital Object Identifier 10.1109/ACCESS.2021.3058734

Reliability and Security Performance Analysis of Hybrid Satellite-Terrestrial Multi-Relay Systems With Artificial Noise

MENGYAN HUANG[1], (Student Member, IEEE), FENGKUI GONG[1], (Member, IEEE), NAN ZHANG[1], GUO LI[1], (Member, IEEE), AND FENG QIAN[2]

[1]State Key Laboratory of Integrated Service Networks, Xidian University, Xi'an 710071, China
[2]School of Communication and Information Engineering, Shanghai University, Shanghai 200444, China

Corresponding author: Nan Zhang (nzhang@xidian.edu.cn)

This work was supported in part by the National Key Research and Development Program of China under Grant 2018YFE0100500, in part by the National Natural Science Foundation of China under Grant 62001354, and in part by the National Natural Science Foundation of Shaanxi Province under Grant 2019CGXNG-010.

ABSTRACT Land mobile satellite communication and physical layer security are considered as the promising paradigms in beyond 5G networks. In this paper, we establish the multi-relay hybrid satellite-terrestrial systems (HSTSs) with artificial noise (AN) to investigate the reliability and security, in which the satellite sends signals to the terrestrial destination through multiple decode-and-forward relays and there exists an eavesdropper trying to overhear the useful information. In order to improve the overall system performance, two relay selection (RS) schemes: *i) optimal relay-receiver pair selection (ORRPS)* and *ii) suboptimal relay selection (SRS)* are considered. ORRPS selects an optimal relay-receiver pair and an AN signal to maximize the corresponding signal-to-interference-plus-noise ratios of $R_k \rightarrow D$ ($R_k \rightarrow E$) and the SRS refers to selecting a relay that optimize the instantaneous channel gain $|h_{R_kD}|^2$ ($|h_{R_kE}|^2$) among K relays, with the *traditional round-robin selection* scheme as a benchmark for comparison. Furthermore, the exact closed-form analytical expressions of outage probability (OP) and intercept probability (IP) under different RS schemes are derived for AN and non-AN conditions. To obtain more insights, the asymptotic analysis for high signal-to-noise-ratio regime is carried out. Based on the asymptotic analysis of OP, the diversity orders of the HSTSs are obtained. The numerical results and theoretical analysis shown that: i) The reliability of TRRS scheme is the worst among the three RS schemes, and the reliability of ORRPS scheme is the best; ii) The AN technology can significantly improve the security of the system, although it has a little adverse affect on the reliability; iii) Infrequent light shadowing has the best reliability, frequent heavy shadowing has the worst outage performance, and the change of security is opposite; iv) The OP of SRS and ORRP schemes decreased with the increase of K, while the IP changed on the contrary, and the reliability and security of TRRS scheme did not change obviously.

INDEX TERMS Land mobile satellite, beyond 5G, physical layer security, artificial noise, reliability-security, relay selection.

I. INTRODUCTION

Land mobile satellite (LMS) communication, as the core of the beyond 5G networks, has attracted a great deal of attention due to its promising characteristics of seamless coverage and high date capacity [1], [2], and it mainly solves the communication tasks of land, sea and between air and ground public networks [3]–[6]. Although LMS communication system has many advantages, it is easy to encounter various security problems due to its inherent broadcast characteristics and large coverage area [7], [8].

Generally, the security issues of LMS systems are realized in the upper layer through encryption schemes [9]–[11]. These traditional information security technologies mainly use authentication and key encryption, which have the possibility of being cracked [11]. To solve this problem, the physical layer security (PLS) firstly proposed by Wyner has become a research focus in the field of information

The associate editor coordinating the review of this manuscript and approving it for publication was Vittorio Camarchia.

security [12]. PLS originated from the perspective of information theory and made full use of the various channel fading characteristics of wireless channels to obtain good security capacity. Among many PLS technologies, i.e., artificial noise (AN) [13]–[15], precoding [16], [17] and beamforming [18], AN has become a hotspot in current researches due to its good compatibility. [13] analyzed the secure performance of the ground system in the presence of AN, and the data information is transmitted from a multi-antenna transmitter to a legitimate user, and there is a malicious single antenna eavesdropper trying to overhear the information. More recently, the system secure performance of the temporal and spatial dimensions with AN was studied in [14], and the analytical expressions of secrecy rate and average secrecy rate were derived. The authors of [15] firstly introduced a data carrying AN based on weighted fractional Fourier transmission to achieve PLS in satellite transmission. From the former research works, we can know that injecting AN into the ground communication systems can reduce the probability of effective information being stolen by potential eavesdroppers. However, there are very few studies on the satellite-terrestrial systems about AN. To narrow the research gap, we establish a PLS model based on satellite-terrestrial transmission to consider the impact of AN on it.

Satellites can provide wireless coverage for geographic areas, where the traditional wired or wireless infrastructures (for example, in the sea) are difficult to deploy. However, in some cases, it is hard to achieve direct links between the satellite and the terrestrial nodes due to so-called masking effects from atmospheric conditions (i.e., clouds, rain, etc.) and ground obstructions (i.e., receivers in tunnels, etc.). To combat these negative effects, the cooperative relay-based hybrid satellite-terrestrial systems (HSTSs) were investigated in literature [19]–[21]. In [19], the future development direction of satellite-terrestrial systems was outlined. A service transmission scheme is proposed that mobile terminals are allowed to forward the signal received from the satellite in [20]. The performance of satellite-terrestrial systems has been analyzed for two relay protocols: i) amplify-and-forward (AF) [22], [23] and ii) decode-and-forward (DF) [21], [24]. Although the target can obtain diversity order gain by using AF protocol, the amplification factor must satisfy the power constraint [25], [26]. Compared with AF, the DF relay only retransmits the correct signals, the number of error bits will be reduced. In this paper, the direct link between the satellite and the ground destination is considered to be impossible because of the existence of heavy fading, and we consider using multiple DF relays to decode the signals sent by the satellite and forward it to the destination.

By sharing the antennas with other mobile users, multiple virtual transmitting antennas can be generated to obtain corresponding diversity gains and improve the performance of the mobile cooperative communication system. Whereas, it generated additional inter-relay interference and energy consumption. To avoid this defect, a few research works about relay selection (RS) schemes were studied for the HSTSs [27]–[32]. Outage probability (OP) was obtained with a max-max user-relay selection scheme, where the secure performance was explored for AF relay protocol with both variable and fixed gains [27]. In [28], the PLS performance was studied for single-relay selection and multi-relay selection strategies with DF relay protocol. Additionally, the authors in [29] investigated the applicability of cognitive radio technology under the integration of relay transmission, and the exact analytical and asymptotic expressions for OP were derived. In [30], [31], a partial RS scheme is investigated and it is used to enhance the system performance by improving the spatial diversity. Based on satellite communication, the RS scheme that minimizes the secure outage probability is proposed in [32]. In order to obtain better quality of service while using AN technology to improve security, the optimal relay-receiver pair selection (ORRPS) and suboptimal relay selection (SRS) [28] schemes are considered in this paper.

A. MOTIVATION AND CONTRIBUTIONS

Inspired by the above discussion, in this paper, the reliability and security of HSTSs based on multi-DF-relay are investigated in the presence of eavesdropper. To further improve the security of the system, AN is used to interfere with the eavesdropper's theft of valid information. The main contributions of this paper are summarized as follows:

- We establish a general PLS framework based on satellite-terrestrial systems in the presence of AN, in which the satellite sends signals to the terrestrial destination through multiple DF terrestrial relays, and there is an eavesdropper trying to intercept valid effective information from satellite and relays.
- The reliability and security are investigated simultaneously for three RS schemes, i.e., ORRPS, SRS, traditional round-robin selection (TRRS) under three channel conditions, i.e., frequent heavy shadowing (FHS), average shadowing (AS) and infrequent light shadowing (ILS). Herein, ORRPS refers to the selection of an optimal relay-receiver pair and an aided AN signal that maximizes the signal-to-interference-plus-noise ratios (SINRs) from relays to the terrestrial receiver, and the SRS is selecting a relay to with the optimal instantaneous channel gain $\left|h_{R_kD}\right|^2$ $\left(\left|h_{R_kE}\right|^2\right)$ of $R_k \rightarrow D/E$. Additionally, two conditions of AN (in presence of AN) and non-AN (in absence of AN) are considered, and the differences in the reliability and security for the three RS schemes of these two cases are studied.
- We derive the exact closed-form analytical expressions of OP and intercept probability (IP) for three RS schemes. To obtain further insights of OP, asymptotic analytical and diversity orders for the HSTSs both AN and non-AN conditions are explored.

B. ORGANIZATION

The rest of this paper is organized as follows. In Section II, we make the description of the HSTSs model, which includes

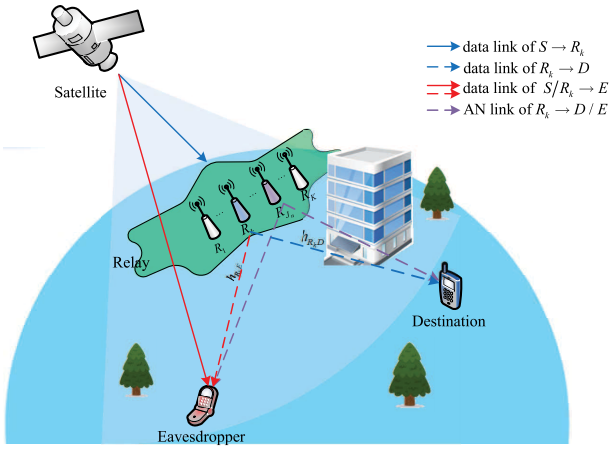

FIGURE 1. Model of multi-relay HSTSs with AN.

the channel model and signal model. Then, the performance analysis of reliability and security is investigated in Section III in terms of OP and IP, respectively. Furthermore, we validate the theoretical analysis in Section IV. Finally, the main conclusions are illustrated in Section V.

C. NOTATION

${}_1F_1(\cdot;\cdot;\cdot)$ is the confluent hypergeometric function of the first kind [33]. $(\cdot)_f$ and $\Gamma(\cdot)$ respectively denote the Pochhammer symbol and gamma function. $f(\cdot)$ and $F(\cdot)$ are the probability density function (PDF) and cumulative distribution function (CDF), respectively. $\mathcal{E}\{\cdot\}$ is expected operator; $|\cdot|$ represents the absolute value and $\Pr\{\cdot\}$ depicts the probability. Otherwise, the $\upsilon_p \sim \mathcal{CN}\left(\mu_p, \sigma_p^2\right)$ is used to illustrate the complex additive white Gaussian noise (AWGN) of mean μ_p and variance σ_p^2.

II. LMS SYSTEM DESCRIPTION

As depicted in Fig. 1, a multi-relay hybrid satellite-terrestrial system is established, which consists of a geostationary orbit regenerative satellite (S), K DF relays R_k ($k \in \{1, 2, \cdots, K\}$), a ground destination (D) and an eavesdropper (E) surrounding the D and it wants to overhear the information from S and R_k. In this paper, all nodes are equipped with a single antenna and they operate in half duplex mode. We think there is no direct links both $S \rightarrow D$ because of the heavy fading and ground obstructions [30], [34][1]. K intermediate nodes are exploited to assist the signal transmission from S to D. The relay nodes are divided into two processes: i) select one relay node R_k to transmit the signal to D and ii) one of the other $K-1$ relay nodes R_{J_n} ($n \in \{1, 2, \cdots, k-1, k+1, \cdots, K\}$) as carrier for emitting AN to prevent E to intercept valid information. To get better system performance, ORRPS and SRS schemes are considered, and TRRS is used as a benchmark for comparison.

The entire communication process can be divided into two phases.

- S transmits its own signal to the R_k;
- R_k decodes and forwards the signal to D or E and one of the residual relays is used to transmit AN to disturb E.

A. CHANNEL MODEL

1) PHASE I

In this subsection, the statistical characterization of the relevant PDF and CDF is illustrated. Herein, the channels of $S \rightarrow R_k$ and $S \rightarrow E$ experience the independent and identically distributed (*i.i.d.*) Shadowed-Rician (SR) fading[2]. The channel coefficient from S to R_k/E, $g_z(z \in \{SR_k, SE\})$ can be expressed as

$$g_z = \mathcal{Q}_z \tilde{g}_z, \tag{1}$$

where $\tilde{g}_z$ represents the channel coefficient following SR fading; $\mathcal{Q}_z$ denotes the scaling parameter that measures the free-space loss (FSL) and on-board beam gain, which is provided by [36]

$$\mathcal{Q}_z = \varpi \sqrt{\frac{\mathcal{G}_{t,z}\mathcal{G}_{r,z}}{\mathcal{K}_{\mathcal{B}}\mathcal{T}\mathcal{B}}}, \tag{2}$$

where $\varpi = \lambda / \left(4\pi d_z'\right)$ denotes the FSL coefficient of one beam and $\lambda = C/f_c$, C and f_c represent the light speed and frequency, respectively; $\mathcal{G}_{t,z}$ and $\mathcal{G}_{r,z}$ are the antenna gain at the satellite and the beam gain of the R_k/E, respectively; d_z' is the distance of propagation; $\mathcal{K}_{\mathcal{B}} = 1.380649 \times 10^{-23} J/K$ and $\mathcal{T}$ respectively are the Boltman constant and the receive noise temperature, in which $\mathcal{B}$ represents the carrier bandwidth.

Based on [37], $\mathcal{G}_{t,z}$ can be obtained as

$$\mathcal{G}_{t,z} = \mathcal{G}_{\max}\left(\frac{J_1(\vartheta)}{2\vartheta} + 36\frac{J_3(\vartheta)}{\vartheta^3}\right)^2, \tag{3}$$

where $\mathcal{G}_{\max}$ is the maximal satellite beam gain and $\vartheta = 2.07123 \sin\theta / \sin\theta_{3dB}$, in which θ is the angle of the corresponding receiver and beam carrier position relative to the S and θ_{3dB} is the $3dB$ angle.

Otherwise, the antenna gain of the earth station for parabolic antenna can be approximately written as [38]

$$\mathcal{G}_{r,z}(dB) \simeq \begin{cases} \bar{\mathcal{G}}_{\max}, 0^\circ < \varphi < 1^\circ \\ 32 - 25\log\varphi, 1^\circ < \varphi < 48^\circ \\ -10, 48^\circ < \varphi \leq 180^\circ, \end{cases} \tag{4}$$

where φ represents the angle of off-boresight; $\bar{\mathcal{G}}_{\max}$ is the maximum beam gain of the boresight.

[1] In some scenarios, destination may receive information from the source and relay, simultaneously. We will consider this assumption in our future work.

[2] Although different fading channel models are proposed for the illustration of statistical models of satellite network channels, SR fading model proposed originally by Loo [35] has found wide applications in characterizing a variety of frequency bands, such as the UHF-band, L-band, S-band and Ka-band [1].

According to [39], the PDF of SR fading can be obtained as

$$f_{|\tilde{g}_z|^2}(x) = \alpha_z e^{-\beta_z x}\, {}_1F_1(m_z; 1; \delta_z x), \quad x \geq 0, \tag{5}$$

where $\tilde{g}_z$ represents the channel coefficient of $S \rightarrow R_k/E$; $\alpha_z = \left(2b_z m_z/(2b_z m_z + \Omega_z)\right)^{m_z}/(2b_z)$, $\delta_z = \Omega_z/(2b_z(2b_z m_z + \Omega_z))$ and $\beta_z = 1/(2b_z)$; Ω_z and $2b_z$ respectively are the average power of line of sight and multiple components; m_z is the fading severity parameter. In fact, the hypergeometric function can be represented via Kummer's transform [39] as

$${}_1F_1(a; b; x) = e^x \sum_{f=0}^{a-b} \frac{(a-b)!x^f}{(a-b-f)!f!(b)_f}, \tag{6}$$

where $(b)_f = b(b+1)\cdots(b+f-1)$ [33]. Thereby, we can simplify ${}_1F_1(m_z; 1; \delta_z x)$ to represent the PDF $f_{|g_z|^2}(x)$ as

$$f_{|\tilde{g}_z|^2}(x) = \alpha_z \sum_{k=0}^{m_z-1} \psi_z(k) x^k e^{-(\beta_z-\delta_z)x}. \tag{7}$$

The CDF can be obtained by integration as

$$\begin{aligned} F_{|\tilde{g}_z|^2}(x) &= \int_{-\infty}^{x} f_{|\tilde{g}_z|^2}(x)dx \\ &= 1 - \alpha_z \sum_{t=0}^{m_z-1} \psi_z(t)(\beta_z - \delta_z)^{-t-1} \\ &\quad \times \Gamma(t+1, (\beta_z - \delta_z)x). \end{aligned} \tag{8}$$

By utilizing the $\Gamma(n,x) = \Gamma(n) - \Upsilon(n,x)$ and $\Upsilon(n,x) = (n-1)![1 - e^{-x}\sum_{d=0}^{n-1}\frac{x^d}{d!}]$ [33], the CDF can be rewritten as (9) at the bottom of next page, where $\psi_z(t) = (-1)^t(1-m_z)_t\delta_z^t/(t!)^2$.

2) PHASE II

Both $R_k \rightarrow D$ and $R_k \rightarrow E$ experience Rayleigh fading and path loss [40], whose CDF and PDF are given, respectively, as

$$F_{|h_j|^2} = 1 - \exp\left(-\lambda_j x\right), \tag{10}$$

$$f_{|h_j|^2} = \lambda_j \exp\left(-\lambda_j x\right), \tag{11}$$

where $\lambda_j\{j \in (R_kD, R_kE)\}$ is the channel parameter of $|h_j|^2$ and $\lambda_j = 1/\mathcal{E}\left\{|h_j|^2\right\}$. In order to better describe the channel path loss, λ_j can be modeled as

$$\lambda_j = d_j^{\tau_j}, \tag{12}$$

where d_j is the link distance from the transmitter to the receiver; $\tau_j\left(2 \leq \tau_j \leq 6\right)$ is the path loss exponent.

B. SIGNAL MODEL

1) PHASE I

In this phase, S transmits the signal to R_k and the legal information is overheard by E, and the received signals at R_k and E can be modeled uniformly as

$$y_z = \sqrt{P_S}\mathcal{Q}_z\tilde{g}_z x_z + \upsilon_z, \tag{13}$$

where P_S is the transmit power of the S; x_z is the received signal from S to z, in which $\mathcal{E}\left[|x_z|^2\right] = 1$.

2) PHASE II

x_{R_kD} is sent to D via DF relay R_k, and the received signal can be expressed as[3]

$$y_{R_kD} = \sqrt{P_{R_k}}h_{R_kD}x_{R_kD} + \sqrt{P_{J_n}}w_{R_{J_n}D} + \upsilon_{R_kD}, \tag{14}$$

where P_{R_k} is the transmit power of R_k and here we set $P_{R_k} = P_S$; h_{R_kD} is the channel coefficient from R_k to D; x_{R_kD} is the received signal of $R_k \rightarrow D$ and $\mathcal{E}\left[\left|x_{R_kD}\right|^2\right]=1$; P_{J_n} denotes the transmit power of AN and $P_{J_n} = aP_{R_k}$, where a represents the allocation coefficient of AN transmit power; $w_{R_{J_n}D}$ is the self-interference signal at D [41]. Hence, the self-interfering signal $w_{R_{J_n}D}$ represents a complex Gaussian random variable with mean zero and variance $\varepsilon_{R_{J_n}D}$, where $\varepsilon_{R_{J_n}D}$ is defined as the self-interfering factor, which is related to CSI when the number of relays is constant.

Meanwhile, E attempts to overhear the decoded signal because of the broadcast nature. Similarly, the received signal at E can be modeled as

$$y_{R_kE} = \sqrt{P_{R_k}}h_{R_kE}x_{R_kE} + \sqrt{P_{J_n}}w_{R_{J_n}E} + \upsilon_{R_kE}, \tag{15}$$

where h_{R_kE} and x_{R_kE} respectively are the channel coefficient and transmit signal of $R_k \rightarrow E$ with $\mathcal{E}\left\{\left|x_{R_kE}\right|^2\right\} = 1$; $w_{R_{J_n}E}$ represents the AN signal at E and it is also a complex Gaussian random variable with mean zero and variance $\varepsilon_{R_{J_n}E}$. $\varepsilon_{R_{J_n}E}$ is defined as AN factor, which is also related to CEEs with the same number of relays.

According to the above modeling analysis, the SINRs of R_k, D and E are, respectively, given by

$$\gamma_z = \frac{P_S\mathcal{Q}_z^2|\tilde{g}_z|^2}{\sigma_z^2}, \tag{16}$$

$$\gamma_{R_kD} = \frac{P_{R_k}\left|h_{R_kD}\right|^2}{P_{J_n}\left|w_{R_{J_n}D}\right|^2 + \sigma_{R_kD}^2}, \tag{17}$$

$$\gamma_{R_kE} = \frac{P_{R_k}\left|h_{R_kE}\right|^2}{P_{J_n}\left|w_{R_{J_n}E}\right|^2 + \sigma_{R_kE}^2}. \tag{18}$$

Therefore, the channel capacities at R_k, D and E based on the Shannon's theorem can be expressed as

$$C_p = \frac{1}{2}\log_2\left(1+\gamma_p\right), \quad p \in \{SR_k, SE, R_kD, R_kE\}. \tag{19}$$

[3]In fact, due to the channel estimation errors (CEEs), AN cannot be designed onto the null space of the vector of main channels exactly, which results in the impact of the AN on D become imperfect.

Since the information is transmitted by two time slots, the penalty factor here is $1/2$ [42], [43].

III. PERFORMANCE ANALYSIS OF RELIABILITY AND SECURITY

In this section, we investigate the reliability and security of the multi-relay HSTSs with DF protocol. The analytical expressions for OP and IP under three RS schemes i.e., TRRS, SRS, and ORRPS are derived, which facilitates the study of effects of different RS schemes and AN.

A. RELIABILITY ANALYSIS

In this subsection, the reliability is investigated and we derive the exact closed-form analytical expressions of OP. To obtain further insights, the asymptotic analysis and diversity orders of OP under high signal-to-noise-ratios (SNRs) $\left(\rho_p = \frac{P_p}{\sigma_p^2} \to \infty\right)$ are studied.

Outage Probability: The definition of OP is that the effective channel capacity of $S \to D$ less than threshold rate C_{th} [30] and it can be expressed as

$$P_{out} \triangleq \Pr\left\{C_{R_k} < C_{th}\right\}, \tag{20}$$

where C_{R_k} is the effective capacity of $S \to D$.

1) TRADITIONAL ROUND-ROBIN SELECTION

The $i-th$ relay is randomly selected among K relays, the effective capacity of $S \to D$ can be expressed as

$$C_{R_i} = \min\left(C_{SR_i}, C_{R_iD}\right). \tag{21}$$

Based on (20) and (21), the exact closed-form expressions of OP for TRRS scheme are given by following **Theorem 1** with AN and non-AN conditions.

Theorem 1: The exact closed-form analytical expressions of OP for TRRS scheme are respectively provided in (22) and (23) under AN and non-AN conditions on the bottom of the next page.

where $\Theta = 2^{2C_{th}} - 1$ and $\Delta_1 = \frac{\Theta\sigma_{SR_i}^2}{P_S Q^2}$.

Proof: See Appendix A. □

To further obtain insights, we study the asymptotic analysis of OP under high SNR region.

Corollary 1: The OP asymptotic expressions of TRRS scheme under high SNR region with AN and non-AN conditions are respectively given by (24) and (25).

- *AN condition*

$$P_{out,TRRS}^{AN,asy} = 1 - \frac{\varepsilon_{R_{J_n}D}}{\varepsilon_{R_{J_n}D} + \lambda_{R_iD} a\Theta}, \tag{24}$$

- *Non-AN condition*

$$P_{out,TRRS}^{Non-AN,asy} = 1 - \left(1 - \alpha_{SR_i}\Delta_1\right)\left(1 - \frac{\lambda_{R_iD}\Theta\sigma_{R_iD}^2}{P_{R_i}}\right). \tag{25}$$

Proof: Under high SNR region, the SINRs of $S \to R_i$ and $R_i \to D$ can be expressed as

$$\gamma_{SR_i}^{\infty} \overset{\rho_{SR_i}\to\infty}{=} \rho_{SR_i}\left|\tilde{g}_{SR_i}\right|^2, \tag{26}$$

$$\gamma_{R_iD}^{\infty} \overset{\rho_{R_iD}\to\infty}{=} \frac{\left|h_{R_iD}\right|^2}{a\left|w_{R_{J_n}D}\right|^2}. \tag{27}$$

Similar to the calculation of OP's exact closed-form expressions for TRRS scheme, (24) can be obtained by utilizing the $\gamma_{SR_i}^{\infty}$ and $\gamma_{R_iD}^{\infty}$.

Under high SNR region, the Maclaurin series expansion as $e^{-z} \underset{z\to 0}{\simeq} 1 - z$ is applied and the asymptotic expressions of PDF and CDF for $\left|\tilde{g}_{SR_i}\right|^2$ and $\left|h_{R_iD}\right|^2$ can be respectively expressed as

$$f_{\left|\tilde{g}_{SR_i}\right|^2}^{\infty}(x) \approx \alpha_{SR_i}, \tag{28}$$

$$F_{\left|\tilde{g}_{SR_i}\right|^2}^{\infty}(x) \approx \alpha_{SR_i} x, \tag{29}$$

$$f_{\left|h_{R_iD}\right|^2}^{\infty}(y) \approx \lambda_{R_iD}, \tag{30}$$

$$F_{\left|h_{R_iD}\right|^2}^{\infty}(y) \approx \lambda_{R_iD} x. \tag{31}$$

According to (A.1) of Appendix A, the asymptotic expression of OP for TRRS scheme under non-AN condition can be obtained as

$$P_{out,TRRS}^{Non-AN,asy} = 1 - \underbrace{\Pr\left\{\frac{P_S\left|\tilde{g}_{SR_i}\right|^2}{\sigma_{SR_i}^2} > \Theta\right\}}_{I_{Non-AN,1}^{asy}} \times \underbrace{\Pr\left\{\frac{P_{R_i}\left|h_{R_iD}\right|^2}{\sigma_{R_iD}^2} > \Theta\right\}}_{I_{Non-AN,2}^{asy}}, \tag{32}$$

where

$$I_{Non-AN,1}^{asy} = 1 - F_{\left|\tilde{g}_{SR_i}\right|^2}^{\infty}(\Delta_1) = 1 - \alpha_{SR_i}\Delta_1, \tag{33}$$

and

$$I_{Non-AN,2}^{asy} = 1 - F_{\left|h_{R_iD}\right|^2}^{\infty}\left(\frac{\Theta\sigma_{R_iD}^2}{P_{R_i}}\right) = 1 - \frac{\lambda_{R_iD}\Theta\sigma_{R_iD}^2}{P_{R_i}}. \tag{34}$$

Substituting (33) and (34) into (32), (25) can be obtained. □

$$F_{|\tilde{g}_z|^2}(x) = 1 - \alpha_z \sum_{t=0}^{m_z-1}\sum_{d=0}^{t}\frac{t!}{d!}\psi_z(t)\left(\beta_z - \delta_z\right)^{-(t+1-d)} x^d e^{-(\beta_z-\delta_z)x}, \tag{9}$$

For further insight, the diversity order of the system is explored, which can be defined as [42]

$$d = -\lim_{\rho_p \to \infty} \frac{\log\left(P_{out}^{asy}\right)}{\log \rho_p}, \tag{35}$$

where ρ_p is the average transmit SNR and P_{out}^{asy} represents the asymptotic expression of OP under high SNR region.

Therefore, according to (24) and (25), we can obtain the diversity orders of TRRS scheme under AN and non-AN conditions showing in following **Corollary 2**.

Corollary 2: The diversity orders of TRRS scheme with AN and non-AN conditions can be provided by

- *AN condition*

$$d_{TRRS}^{AN} = 0, \tag{36}$$

- *Non-AN condition*

$$d_{TRRS}^{Non-AN} = 1. \tag{37}$$

Proof: Substituting (24) into (35), (36) is equal to 0 due to the fact that $P_{out,TRRS}^{AN,asy}$ is a constant.

By putting (25) into (35), the following calculation process can be obtained as

$$\begin{aligned} d_{TRRS}^{Non-AN} &= -\lim_{\rho \to \infty} \frac{\log\left(\frac{\alpha_{SR_i}\Theta + \lambda_{R_iD}\Theta - \alpha_{SR_i}\lambda_{R_iD}\Theta^2}{\rho}\right)}{\log \rho} \\ &= -\lim_{\rho \to \infty} \frac{\log\left(\alpha_{SR_i} + \lambda_{R_iD} - \alpha_{SR_i}\lambda_{R_iD}\Theta\right) - \log \rho}{\log \rho} \\ &= 1, \end{aligned} \tag{38}$$

where $\rho = P_S \Big/ \sigma_{SR_i}^2 = P_{R_i} \Big/ \sigma_{R_iD}^2$, and (37) can be obtained. □

*Remark 1: From **Theorem 1**, **Corollary 1** and **Corollary 2**, it can be observed that the outage performance of the systems for TRRS scheme gradually becomes better with the increases of transmit power, and the OP for AN condition tends to a constant under high SNR region, that is, there exists an error floor. Otherwise, we can obtain that when the number of relays increases, the reliability under TRRS scheme with AN and non-AN conditions is not affected by the number of relays.*

2) SUBOPTIMAL RELAY SELECTION

The $b-th$ relay is selected to maximize the instantaneous channel gain of $R_k \rightarrow D$ among K relays, the relative expressions can be expressed as

$$b = \arg \max_{k \in \{1,2,\cdots,K\}} \left|h_{R_kD}\right|^2, \tag{39}$$

$$C_{R_b} = \min\left(C_{SR_b}, C_{R_bD}\right). \tag{40}$$

For SRS scheme, the CDF of $\left|h_{R_bD}\right|^2$ can be obtained as

$$F_{\left|h_{R_bD}\right|^2}(x) = \left[1 - e^{-\lambda_{R_bD}x}\right]^K. \tag{41}$$

By taking the derivative of above CDF, the PDF can be shown as

$$f_{\left|h_{R_bD}\right|^2}(x) = K \sum_{l_1=0}^{K-1} \binom{K-1}{l_1} (-1)^{l_1} \lambda_{R_bD} e^{-\lambda_{R_bD}(l_1+1)x}. \tag{42}$$

The exact analytical expressions of OP for AN and non-AN conditions can be provided in **Theorem 2** by utilizing (20) and (40).

Theorem 2: The exact closed-form analytical expressions of OP for SRS scheme are respectively provided in (43) and (44) under AN and non-AN conditions on the bottom of the next page.

where $\Delta_2 = \frac{\Theta\sigma_{SR_b}^2}{P_S Q^2}$.

Proof: See Appendix B. □

To further investigate the outage performance for SRS scheme, the asymptotic analysis of OP are derived as following **Corollary 3**.

Corollary 3: The OP asymptotic expressions for SRS scheme under high SNR region with AN and non-AN conditions are respectively given by (45) and (46).

- *AN condition*

$$P_{out,SRS}^{AN,asy} = \sum_{l_1=0}^{K} \binom{K}{l_1} (-1)^{l_1} \frac{\varepsilon_{R_{J_n}D}}{\varepsilon_{R_{J_n}D} + l_1 \lambda_{R_bD} a\Theta}, \tag{45}$$

- *Non-AN condition*

$$\begin{aligned} P_{out,SRS}^{Non-AN,asy} &= 1 - \left(1 - \alpha_{SR_b}\Delta_2\right) \\ &\quad \times \left(1 - \left(\frac{\lambda_{R_bD}\Theta\sigma_{R_bD}^2}{P_{R_b}}\right)^K\right). \end{aligned} \tag{46}$$

$$\begin{aligned} P_{out,TRRS}^{AN} &= 1 - \left[\alpha_{SR_i} \sum_{t=0}^{m_{SR_i}-1} \sum_{d=0}^{t} \psi_{SR_i}(t) \left(\beta_{SR_i} - \delta_{SR_i}\right)^{-(t+1-d)} \frac{t!}{d!} \Delta_1{}^d e^{-\left(\beta_{SR_i} - \delta_{SR_i}\right)\Delta_1}\right] \\ &\quad \times \left(\frac{\varepsilon_{R_{J_n}D} P_{R_i}}{\varepsilon_{R_{J_n}D} P_{R_i} + \lambda_{R_iD}\Theta P_{J_n}} e^{-\frac{\lambda_{R_iD}\Theta\sigma_{R_iD}^2}{P_{R_i}}}\right), \end{aligned} \tag{22}$$

$$P_{out,TRRS}^{Non-AN} = 1 - \left[\alpha_{SR_i} \sum_{t=0}^{m_{SR_i}-1} \sum_{d=0}^{t} \psi_{SR_i}(t) \left(\beta_{SR_i} - \delta_{SR_i}\right)^{-(t+1-d)} \frac{t!}{d!} \Delta_1{}^d e^{-\left(\beta_{SR_i} - \delta_{SR_i}\right)\Delta_1}\right] e^{-\frac{\lambda_{R_iD}\Theta\sigma_{R_iD}^2}{P_{R_i}}}. \tag{23}$$

Proof: The SINRs of $S \to R_b$ and $R_b \to D$ under high SNR region are similar to (26) and (27).

Similar to the calculation of OP for SRS scheme, (45) can be obtained.

According the similar asymptotic process of TRRS scheme, the asymptotic expressions of PDF and CDF for $\left|\tilde{g}_{SR_b}\right|^2$ and $\left|h_{R_bD}\right|^2$ are similar to (28)-(31).

Based on the calculation of Appendix B, the $I^{asy}_{Non-AN,4}$ and $I^{asy}_{Non-AN,4}$ can be obtained as

$$I^{asy}_{Non-AN,3} = 1 - F^{\infty}_{\left|\tilde{g}_{SR_b}\right|^2}(\Delta_2) = 1 - \alpha_{SR_b}\Delta_2, \quad (47)$$

and

$$I^{asy}_{Non-AN,4} = 1 - F^{\infty}_{|h_{R_bD}|^2}\left(\frac{\Theta\sigma^2_{R_bD}}{P_{R_b}}\right) = 1 - \frac{\lambda_{R_bD}\Theta\sigma^2_{R_bD}}{P_{R_b}}. \quad (48)$$

By substitution operations similar to those in Appendix B, (46) can be obtained. □

Based on (35), the diversity orders of SRS scheme can be calculated as the following **Corollary 4**.

Corollary 4: The diversity orders of SRS scheme with AN and non-AN conditions can be provided by

- *AN condition*

$$d^{AN}_{SRS} = 0, \quad (49)$$

- *Non-AN condition*

$$d^{Non-AN}_{SRS} = 1. \quad (50)$$

Proof: Since the $P^{AN,asy}_{out,SRS}$ is a non-zero constant, (49) can be obtained by the definition.

Similar to the calculation process of **Corollary 2**, (50) can be obtained by using L'Hospital's rule. □

*Remark 2: We found from **Theorem 2** and **Corollary 3** that the reliability for SRS scheme decreases as K increases. From (45), the increases of the self-interfering of $R_n \to D$ promotes the OP of the systems. In addition, it can be observed from (43) and (45) that the reliability will be destroyed when the threshold rate increases. The diversity order of (50) is one, which indicates that the diversity gain will not be affected when using SRS scheme.*

3) OPTIMAL RELAY-RECEIVER PAIR SELECTION

In this subsection, we consider the scenario where the ORRPS selects an optimal relay-receiver pair and an AN signal to maximize the corresponding SINRs of $R_k \to D$. Therefore, the following expression is obtained as

$$\{o, n*\} = \arg \max_{i\in\{1,\cdots,K\}} \max_{n\in\{1,\cdots,i-1,i+1,\cdots,K\}} \times \frac{P_{R_i}\left|h_{R_iD}\right|^2}{P_{J_n}\left|w_{R_{J_n}D}\right|^2 + \sigma^2_{R_iD}}, \quad (51)$$

$$C_{R_o} = \min\left(C_{SR_o}, C_{R_oD}\right). \quad (52)$$

Based on (20) and (52), we can obtain the closed-form analytical expressions of OP for ORRPS scheme by considering AN and non-AN conditions in the following **Theorem 3**.

Theorem 3: The exact closed-form analytical expressions of OP for ORRPS scheme are respectively provided in (53) and (54) under AN and non-AN conditions on the bottom of the next page.

Proof: See Appendix C. □

To further study the performance of systems, we derive the asymptotic expressions of the ORRPS scheme showing in the following **Corollary 5**.

Corollary 5: The OP asymptotic expressions for ORRPS scheme under high SNR region with AN and non-AN conditions are respectively given by (55) and (56).

- *AN condition*

$$P^{AN,asy}_{out,ORRPS} = 1 - \left(\frac{\varepsilon_{R_{J_n}D}}{\varepsilon_{R_{J_n}D} + \lambda_{R_mD}a\Theta}\right)^K, \quad (55)$$

- *Non-AN condition*

$$P^{Non-AN,asy}_{out,ORRPS} = 1 - \left(1 - \alpha_{SR_i}\Delta_1\right) \times \left(1 - \left(\frac{\lambda_{R_iD}\Theta\sigma^2_{R_iD}}{P_{R_i}}\right)^K\right). \quad (56)$$

Based (35), the diversity orders of ORRPS scheme can be calculated as the following **Corollary 6**.

Corollary 6: The diversity orders of ORRPS scheme with AN and non-AN conditions can be provided by

$$P^{AN}_{out,SRS} = 1 - \left(\alpha_{SR_b}\sum_{t=0}^{m_{SR_b}-1}\sum_{d=0}^{t}\psi_{SR_b}(t)\left(\beta_{SR_b} - \delta_{SR_b}\right)^{-(t+1-d)}\frac{t!}{d!}\Delta_2{}^d e^{-\left(\beta_{SR_b}-\delta_{SR_b}\right)\Delta_2}\right) \times \left(1 - \sum_{l_1=0}^{K}\binom{K}{l_1}(-1)^{l_1}\frac{\varepsilon_{R_{J_n}D}P_{R_b}}{\varepsilon_{R_{J_n}D}P_{R_b} + l_1\lambda_{R_bD}\Theta P_{J_n}}e^{-\frac{l_1\lambda_{R_bD}\Theta\sigma^2_{R_bD}}{P_{R_b}}}\right), \quad (43)$$

$$P^{Non-AN}_{out,SRS} = 1 - \left(\alpha_{SR_b}\sum_{t=0}^{m_{SR_b}-1}\sum_{d=0}^{t}\psi_{SR_b}(t)\left(\beta_{SR_b} - \delta_{SR_b}\right)^{-(t+1-d)}\frac{t!}{d!}\Delta_2{}^d e^{-\left(\beta_{SR_b}-\delta_{SR_b}\right)\Delta_2}\right) \times \left(1 - \sum_{l_1=0}^{K}\binom{K}{l_1}(-1)^{l_1}e^{-\frac{l_1\lambda_{R_bD}\Theta\sigma^2_{R_bD}}{P_{R_b}}}\right). \quad (44)$$

- *AN condition*

$$d_{ORRPS}^{AN} = 0, \tag{57}$$

- *Non-AN condition*

$$d_{ORRPS}^{Non-AN} = 1. \tag{58}$$

Proof: Similar to the calculation of **Corollary 3** and **Corollary 4**, (55)-(58) can be derived. □

*Remark 3: According to the **Theorem 3**, **Corollary 5** and **Corollary 6**, it can be seen that when the number of relays increases, the OP of ORRPS scheme becomes smaller, which means that the OP's error floor for AN condition will be lower as K rises. Finally, we found the diversity order of ORRPS scheme under non-AN condition is one, which is the same as for SRS and TRRS scheme.*

B. SECURITY ANALYSIS

In this subsection, the security of multi-relay HSTSs with two conditions of AN and non-AN is investigated. Additionally, the closed-form analytical expressions of IP are derived by considering three RS strategies.

Intercept Probability: Based on [42], the IP of the system is defined that the channel capacity of R_k to E is greater than threshold rate C_{th}, and it can be written as

$$P_{int} = \Pr\{C_E > C_{th}\}, \tag{59}$$

where C_{R_kE} is the channel capacity of $R_k \to E$.

1) TRADITIONAL RANDOM RELAY SELECTION

Herein, we randomly select i-relay among K relays, the maximum reachability capacity received by the eavesdropper from S and R_k under the assumption of the selection combining (SC) can be expressed as

$$C_E^i = \max\left\{C_{SE}, C_{R_iE}\right\}. \tag{60}$$

According to (59) and (60), the following theorem shows the exact closed-form analytical expressions of IP for TRRS strategy under AN and non-AN conditions.

Theorem 4: The exact closed-form analytical expressions of IP for TRRS strategy are respectively provided in (61) and (62) under AN and non-AN conditions on the bottom of the next page.

where $\Delta_4 = \frac{\Theta\sigma_{SE}^2}{P_S Q^2}$.

Proof: See Appendix D-1). □

2) SUBOPTIMAL RELAY SELECTION

The $c-th$ relay is selected to optimize the instantaneous eavesdrop channel gain, and it can be modeled as

$$c = \arg\max_{k=1,2,\cdots,K} \left|h_{R_kE}\right|^2. \tag{63}$$

Similar to (60), the eavesdrop capacity for SRS scheme can be shown as

$$C_E^c = \max\left\{C_{SE}, C_{R_cE}\right\}. \tag{64}$$

For SRS strategy, the CDF and PDF for $\left|h_{R_cE}\right|^2$ are similar to (41) and (42).

Based on (59) and (64), the IP expressions for SRS strategy with AN and non-AN conditions are given by **Theorem 5**.

Theorem 5: The exact closed-form analytical expressions of IP for SRS strategy are respectively provided in (65) and (66) under AN and non-AN conditions on the bottom of the next page.

Proof: See Appendix D-2). □

3) OPTIMAL RELAY-RECEIVER PAIR SELECTION

The $g-th$ relay-receiver pair and $n' - th$ AN signal are selected to maximize the eavesdrop channel SINR, and corresponding expressions can be written as

$$\left\{g, n'\right\} = \arg\max_{i\in\{1,\cdots,K\}} \max_{n\in\{1,\cdots,i-1,i+1,\cdots,K\}} \times \frac{P_{R_i}\left|h_{R_iE}\right|^2}{P_{J_n}\left|w_{R_{J_n}E}\right|^2 + \sigma_{R_iE}^2}, \tag{67}$$

$$C_E^g = \max\left\{C_{SE}, C_{R_gE}\right\}. \tag{68}$$

According to (59) and (67), the exact closed-form IP expressions for ORRPS strategy with AN and non-AN conditions can be shown in **Theorem 6**.

Theorem 6: The exact closed-form analytical expressions of IP for ORRPS strategy are respectively provided in (69) and (70) under AN and non-AN conditions on the bottom of the next page.

Proof: See Appendix D-3). □

$$P_{out,ORRPS}^{AN} = 1 - \left(\alpha_{SR_o} \sum_{t=0}^{m_{SR_o}-1} \sum_{d=0}^{t} \psi_{SR_o}(t) \left(\beta_{SR_o} - \delta_{SR_o}\right)^{-(t+1-d)} \frac{t!}{d!} {\Delta_1}^d e^{-(\beta_{SR_o}-\delta_{SR_o})\Delta_1}\right) \times \left(1 - \prod_{k=1}^{K}\left(1 - \frac{\varepsilon_{R_{J_n}D} P_{R_i}}{\varepsilon_{R_{J_n}D} P_{R_i} + \lambda_{R_iD}\Theta P_{J_n}} e^{-\frac{\lambda_{R_iD}\Theta\sigma_{R_iD}^2}{P_{R_i}}}\right)\right), \tag{53}$$

$$P_{out,ORRPS}^{Non-AN} = 1 - \left(\alpha_{SR_o} \sum_{t=0}^{m_{SR_o}-1} \sum_{d=0}^{t} \psi_{SR_o}(t) \left(\beta_{SR_o} - \delta_{SR_o}\right)^{-(t+1-d)} \frac{t!}{d!} {\Delta_1}^d e^{-(\beta_{SR_o}-\delta_{SR_o})\Delta_1}\right) \left(1 - \prod_{k=1}^{K}\left(1 - e^{-\frac{\lambda_{R_iD}\Theta\sigma_{R_iD}^2}{P_{R_i}}}\right)\right). \tag{54}$$

TABLE 1. System parameters [44].

Monte Carlo simulation iteration	10^6
Frequency band	$f = 2GHz$
Link bandwidth	$\mathcal{B} = 15MHz$
Noise temperature	$\mathcal{T} = 300^\circ K$
3dB angle	$\varphi_{3dB} = 0.8^\circ$
Maximal beam gain	$\mathcal{G}_{\max} = 48dB$
Receive gain from satellite to receiver	$\mathcal{G}_{r,z} = 4dB$
The allocation coefficient of AN factor	$a = 0.1$
Relay number	$K = 3$
Link distance from transmitter to receiver	$d_j = 1.5m$
Path loss exponent	$\tau_j = 3$
Noise power	$\sigma_i^2 = 1$
Threshold rate	$C_{th} = 1$
Random number distribution range	$range \in [0, 1]$
Self-interfering factor of $R_n \to D$	$\varepsilon_{R_{J_n}D} = 0.1$
AN factor of $R_n \to E$	$\varepsilon_{R_{J_n}E} = 0.9$
Fading severity parameter	$m_z = 2$
Multiple component	$b_z = 0.063$
Average power of line of sight	$\Omega_z = 0.0007$

TABLE 2. Channel parameters [37], [44].

Shadowing	Case	m_z	b_z	Ω_z
Frequent heavy shadowing (FHS)	I	2	0.063	0.0007
Frequent heavy shadowing (FHS)	II	1.95	0.063	0.0007
Average shadowing (AS)	I	5	0.251	0.0007
Average shadowing (AS)	II	4.95	0.251	0.0007
Infrequent light shadowing (ILS)	I/II	10	0.158	1.29

*Remark 4: From **Theorem 4**, **Theorem 5** and **Theorem 6**, we can obtain that: i) The IP for ORRPS strategy is larger than the SRS and TRRS strategies, which proves that its security is the worst; ii) According to (61) and (62), the security for TRRS strategy is not be affected the number of relays; iii) The security for strategies SRS and ORRPS deteriorates as the K increases.*

IV. NUMERICAL RESULTS

In this section, we validate the correctness of theoretical analysis in Section III by simulating some numerical results. The parameters are shown in Table 1 and Table 2 unless otherwise specified.

$$P_{int,TRRS}^{AN} = 1 - \left(1 - \alpha_{SE} \sum_{t=0}^{m_{SE}-1} \sum_{d=0}^{t} \psi_{SE}(t) (\beta_{SE} - \delta_{SE})^{-(t+1-d)} \frac{t!}{d!} \Delta_4{}^d e^{-(\beta_{SE}-\delta_{SE})\Delta_4}\right) \times \left(1 - \frac{\varepsilon_{R_{J_n}E} P_{R_i}}{\varepsilon_{R_{J_n}E} P_{R_i} + \lambda_{R_iE}\Theta P_{J_n}} e^{-\frac{\lambda_{R_iE}\Theta\sigma_{R_iE}^2}{P_{R_i}}}\right), \tag{61}$$

$$P_{int,TRRS}^{Non-AN} = 1 - \left(1 - \alpha_{SE} \sum_{t=0}^{m_{SE}-1} \sum_{d=0}^{t} \psi_{SE}(t) (\beta_{SE} - \delta_{SE})^{-(t+1-d)} \frac{t!}{d!} \Delta_4{}^d e^{-(\beta_{SE}-\delta_{SE})\Delta_4}\right) \left(1 - e^{-\frac{\lambda_{R_iE}\Theta\sigma_{R_iE}^2}{P_{R_i}}}\right). \tag{62}$$

$$P_{int,SRS}^{AN} = 1 - \left(1 - \alpha_{SE} \sum_{t=0}^{m_{SE}-1} \sum_{d=0}^{t} \psi_{SE}(t) (\beta_{SE} - \delta_{SE})^{-(t+1-d)} \frac{t!}{d!} \Delta_4{}^d e^{-(\beta_{SE}-\delta_{SE})\Delta_4}\right) \times \sum_{f=0}^{K} \binom{K}{f} \frac{(-1)^f \varepsilon_{R_{J_n}E} P_{R_c}}{P_{R_c}\varepsilon_{R_{J_n}E} + f\lambda_{R_cE}\Theta P_{J_n}} e^{-\frac{f\lambda_{R_cE}\Theta\sigma_{R_cE}^2}{P_{R_c}}}, \tag{65}$$

$$P_{int,SRS}^{Non-AN} = 1 - \left(1 - \alpha_{SE} \sum_{t=0}^{m_{SE}-1} \sum_{d=0}^{t} \psi_{SE}(t) (\beta_{SE} - \delta_{SE})^{-(t+1-d)} \frac{t!}{d!} \Delta_4{}^d e^{-(\beta_{SE}-\delta_{SE})\Delta_4}\right) \sum_{f=0}^{K} \binom{K}{f} (-1)^f e^{-\frac{f\lambda_{R_cE}\Theta\sigma_{R_cE}^2}{P_{R_c}}}. \tag{66}$$

$$P_{int,ORRPS}^{AN} = 1 - \left(1 - \alpha_{SE} \sum_{t=0}^{m_{SE}-1} \sum_{d=0}^{t} \psi_{SE}(t) (\beta_{SE} - \delta_{SE})^{-(t+1-d)} \frac{t!}{d!} \Delta_4{}^d e^{-(\beta_{SE}-\delta_{SE})\Delta_4}\right) \times \prod_{k=1}^{K} \left(1 - \frac{\varepsilon_{R_{J_n}E} P_{R_i}}{\varepsilon_{R_{J_n}E} P_{R_i} + \lambda_{R_iE}\Theta P_{J_n}} e^{-\frac{\lambda_{R_iE}\Theta\sigma_{R_iE}^2}{P_{R_i}}}\right), \tag{69}$$

$$P_{int,ORRPS}^{Non-AN} = 1 - \left(1 - \alpha_{SE} \sum_{t=0}^{m_{SE}-1} \sum_{d=0}^{t} \psi_{SE}(t) (\beta_{SE} - \delta_{SE})^{-(t+1-d)} \frac{t!}{d!} \Delta_4{}^d e^{-(\beta_{SE}-\delta_{SE})\Delta_4}\right) \prod_{k=1}^{K} \left(1 - e^{-\frac{\lambda_{R_iE}\Theta\sigma_{R_iE}^2}{P_{R_i}}}\right). \tag{70}$$

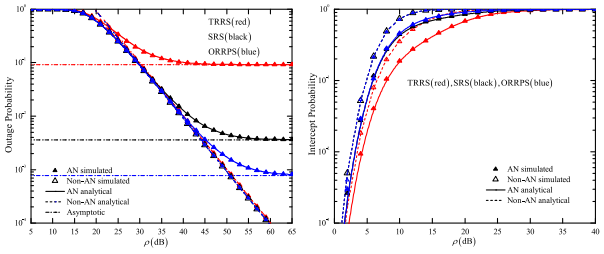

(a) (b)

FIGURE 2. Influence of different RS schemes: (a) OP versus ρ for AN and non-AN conditions; (b) IP versus ρ for AN and non-AN conditions.

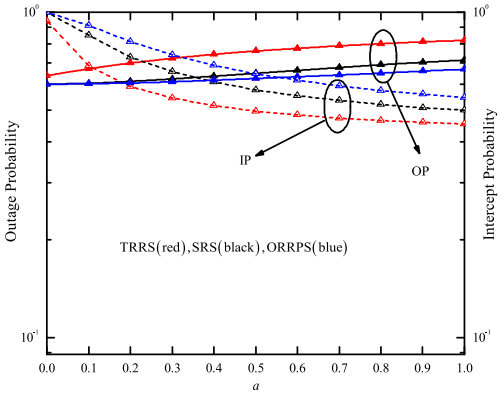

FIGURE 3. OP and IP versus a for different RS schemes.

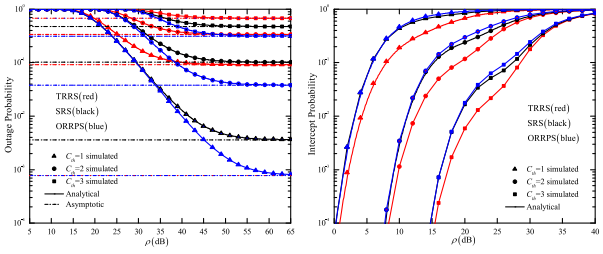

(a) (b)

FIGURE 4. Influence of different C_{th}: (a) OP versus ρ under three RS schemes; (b) IP versus ρ under three RS schemes.

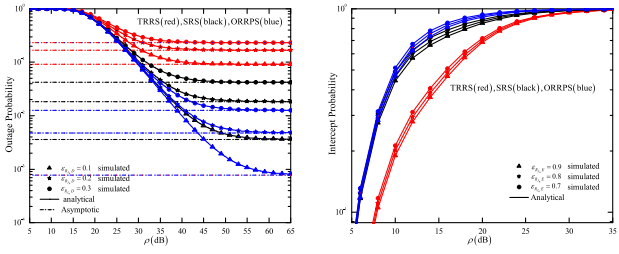

(a) (b)

FIGURE 5. Influence of different $\varepsilon_{R_{J_n}D}/\varepsilon_{R_{J_n}E}$: (a) OP versus ρ under three RS schemes; (b) IP versus ρ under three RS schemes.

Fig. 2(a) and Fig. 2(b) respectively show the OP and IP versus ρ for different RS schemes. In this simulation, we considering two conditions: i) AN condition: $a = 0.1$ and ii) non-AN condition: $a = 0$. In Fig. 2(a), these simulated curves verify our theoretical analysis of OP in Section III, it is found that the outage performance gradually becomes stronger as ρ increases. Through comparison, it is shown that the outage performance for TRRS scheme is worse than the SRS scheme when the system exists AN, and the ORRPS scheme has the best outage performance among three RS schemes; This situation occurs since that compared with the TRRS scheme, the system will obtain better transmission quality of service under other two schemes. However, we can see from Fig. 2(b) that the IP for TRRS strategy is smaller than the SRS strategy, and the IP under ORRPS strategy is the largest and it verifies the correctness of analytical expressions for IP in Section III. Additionally, the OP and IP under the SRS and ORRPS strategies do not change significantly when there is no AN. Furthermore, it can be observed that the OP of AN condition is higher than non-AN condition and the IP changes are the opposite. Moreover, there are error floors of OP for three RS schemes under high SNR region in the presence of AN, the (36), (49) and (57) in Section III are verified. When there is no self-interference of $R_n \rightarrow D$, the slopes of asymptotic OP are not zero, which verifies the analysis of (37), (50) and (58) in Section III; This indicates that the AN has a very negative impact on the outage performance of the system.

In Fig. 3, the OP and IP versus $a \in [0, 1]$ for different RS schemes are studied, where $\rho = 20dB$. We can conclude that it will promote OP to become larger when the systems increases the power allocation coefficient of AN. In contrast, an enhanced IP is achieved with the decrease of a. This simulation further verified some of the conclusions in Fig. 2, i.e., the reliability becomes stronger with TRRS, SRS and ORRPS, but the security situation is completely the opposite.

Fig. 4(a) and Fig. 4(b) illustrate the OP and IP versus ρ for different $C_{th} = \{1, 2, 3\}$, respectively. In Fig. 4(a), we can observe that the reliability of systems for three RS schemes becomes worsen with the increase of threshold rate. By contrast, the changes in security are robust as the enlargement of C_{th} in Fig. 4(b). The main reason for this is that the effective channel capacity of $S \rightarrow D$ is less than its increasing threshold rate, but the variation of the eavesdrop capacity of the system is the opposite. Finally, there are error floors of OP under high SNR region and it is corresponding to Fig. 2.

Fig. 5(a) and Fig. 5(b) investigate the OP and IP under RS schemes versus ρ for different $\left(\varepsilon_{R_{J_n}D}, \varepsilon_{R_{J_n}E}\right) = \{(0.1, 0.9)\,; (0.2, 0.8)\,; (0.3, 0.7)\}$, respectively. Herein, we set $K = 3$. This simulation illustrates that the OPs for three RS schemes are improved as the self-interfering factor of $R_n \rightarrow D$ increases and the AN factor of $R_n \rightarrow E$ has a negative effect on the IPs. We can also draw the conclusion that by increasing the AN factor can improve the security, but it will also have a small negative impact on reliability.

Fig. 6(a) and Fig.6(b) respectively present the OP and IP under RS schemes versus ρ for different shadowing scenarios, i.e., FHS, AS and ILS, where $K = 3$. We observe that the reliability and security are sensitive to the shadowing condition of satellite-terrestrial channels. Several conclusions

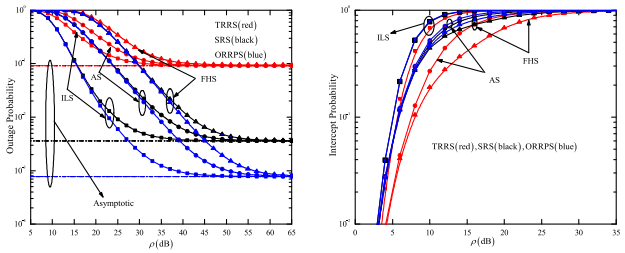

(a) (b)

FIGURE 6. Case II: Influence of different shadowing: (a) OP versus ρ under three RS schemes; (b) IP versus ρ under three RS schemes.

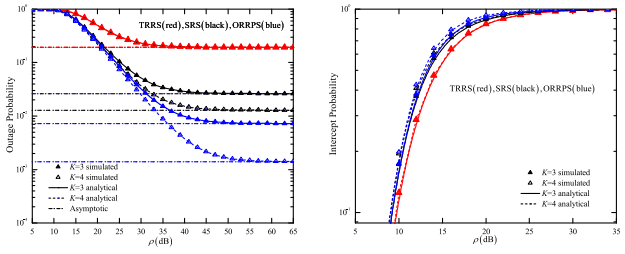

(a) (b)

FIGURE 7. Influence of different K: (a) OP versus ρ under three RS schemes; (b) IP versus ρ under three RS schemes.

can be obtained as: i) FHS will lead to lower reliability of the system, and ILS of the three shadowing methods will make the best reliability, since the higher shadowing severities correspond to worse propagation conditions; ii) The security changes in the three shadowing conditions are opposite to the reliability; iii) In high SNR case, OP in the same RS schemes tends to a fixed error floor, that is, the reliability of the systems is stable when the SNRs are high enough.

Fig. 7(a) and Fig. 7(b) respectively depict the OP and IP under RS schemes versus ρ for different number of the relays $K = \{3, 4\}$. Herein, the other parameters are $(m_z, b_z, \Omega_z) = (5, 0.251, 0.0007)$ and $d_j = 2m$. Fig. 7(a) shows the whole reliability becomes better when K rises. Furthermore, it can be drawn that the systems for ORRPS scheme can achieve better reliability than that SRS scheme by increasing the number of relays. Additionally, the security of SRS and ORRPS schemes is worse with K increases in Fig. 7(b), while it will gradually stabilize as SNR becomes higher. We can also seen that the reliability and security for TRRS scheme remain basically unchanged.

V. CONCLUSION

In this paper, we not only studied the performance difference for different RS schemes, i.e., TRRS, SRS and ORRPS, but also investigated the impact of AN on the reliability and security of the proposed HSTSs. Through further modeling and analysis, the exact closed-form expressions about OP and IP based on diverse RS schemes are derived. To obtain more useful knowledge, we further calculated the expressions of asymptotic analysis and diversity order for OP under high SNR region. The numerical results and theoretical analysis shown that: i) the reliability under TRRS scheme is worse than SRS scheme, and the reliability of ORRPS scheme is the best among three RS schemes, and security varies under the three RS strategies as opposed to reliability; ii) Although the system may adversely affect the reliability of the system when using AN technology, it will greatly improve the security of the system; iii) Reliability in the case of ILS is the best, but it will cause the worst outage performance when in the case of FHS, and the change in security is the opposite; iv) As the number of relays increases, the OP will reduce and the change of IP is opposite for SRS and ORRPS schemes, and the changing states of reliability and security for TRRS scheme are not obvious.

.

APPENDIX A PROOF OF THEOREM 1

Substituting (21) into (20), the following expression can be obtained as

$$P_{out,TRRS}^{AN} = 1 - \underbrace{\Pr\left\{\frac{P_S\left|\tilde{g}_{SR_i}\right|^2}{\sigma_{SR_i}^2} > \Theta\right\}}_{I_1} \times \underbrace{\Pr\left\{\frac{P_{R_i}\left|h_{R_iD}\right|^2}{P_{J_n}\left|w_{R_{J_n}D}\right|^2 + \sigma_{R_iD}^2} > \Theta\right\}}_{I_2}, \quad \text{(A.1)}$$

where

$$I_1 = 1 - \Pr\left\{\frac{P_S\left|\tilde{g}_{SR_i}\right|^2}{\sigma_{SR_i}^2} < \Theta\right\} = 1 - F_{\left|\tilde{g}_{SR_i}\right|^2}(\Delta_1). \quad \text{(A.2)}$$

Based on (9), I_1 can be calculated as

$$I_1 = \alpha_{SR_i} \sum_{t=0}^{m_{SR_i}-1} \psi_{SR_i}(t)\left(\beta_{SR_i} - \delta_{SR_i}\right)^{-(t+1-d)} \times \sum_{d=0}^{t} \frac{t!}{d!}\Delta_1{}^d e^{-\left(\beta_{SR_i}-\delta_{SR_i}\right)\Delta_1}, \quad \text{(A.3)}$$

and

$$I_2 = 1 - \int_0^{\infty} f_{\left|w_{R_{J_n}D}\right|^2}(x) \int_0^{\frac{\Theta P_{J_n} x + \Theta\sigma_{R_iD}^2}{P_{R_i}}} f_{\left|h_{R_iD}\right|^2}(y)\, dydx. \quad \text{(A.4)}$$

Putting (11) into (A.4), I_2 can be obtained as

$$I_2 = \frac{\varepsilon_{R_{J_n}D} P_{R_i}}{\varepsilon_{R_{J_n}D} P_{R_i} + \lambda_{R_iD}\Theta P_{J_n}} e^{-\frac{\lambda_{R_iD}\Theta\sigma_{R_iD}^2}{P_{R_i}}}. \quad \text{(A.5)}$$

According to (A.3) and (A.5), we can derive the (22).

When the allocation coefficient of AN power is 0, that is, $a = 0$, (23) can be obtained.

APPENDIX B PROOF OF THEOREM 2

By utilizing (20), (40) and the similar process of Appendix A, where

$$\begin{aligned} I_3 &= 1 - F_{\left|\tilde{g}_{SR_b}\right|^2}(\Delta_2) \\ &= \alpha_{SR_b} \sum_{t=0}^{m_{SR_b}-1} \psi_{SR_b}(t) \left(\beta_{SR_b} - \delta_{SR_b}\right)^{-(t+1-d)} \\ &\quad \times \sum_{d=0}^{t} \frac{t!}{d!} \Delta_2{}^d e^{-\left(\beta_{SR_b} - \delta_{SR_b}\right)\Delta_2}, \end{aligned} \tag{B.1}$$

and

$$I_4 = 1 - \int_0^{\infty} f_{\left|w_{R_{J_n}D}\right|^2}(x) F_{\left|h_{R_bD}\right|^2}\left(\frac{\Theta P_{J_n} x + \Theta \sigma_{R_bD}^2}{P_{R_b}}\right) dx. \tag{B.2}$$

Substituting (11) and (42) into (B.2), I_4 can be further obtained as

$$\begin{aligned} I_4 = 1 - \sum_{l_1=0}^{K} \binom{K}{l_1} (-1)^{l_1} \frac{\varepsilon_{R_{J_n}D} P_{R_b}}{\varepsilon_{R_{J_n}D} P_{R_b} + l_1 \lambda_{R_bD} \Theta P_{J_n}} \\ \times e^{-\frac{l_1 \lambda_{R_bD} \Theta \sigma_{R_bD}^2}{P_{R_b}}}. \end{aligned} \tag{B.3}$$

We can get (43) by using (B.1) and (B.3).

When a is equal to zero, (44) can be derived.

APPENDIX C PROOF OF THEOREM 3

Putting (52) into (20), the derivation is similar to Appendix A, where

$$\begin{aligned} I_5 &= 1 - F_{\left|\tilde{g}_{SR_o}\right|^2}(\Delta_3) \\ &= \alpha_{SR_o} \sum_{t=0}^{m_{SR_o}-1} \psi_{SR_o}(t) \left(\beta_{SR_o} - \delta_{SR_o}\right)^{-(t+1-d)} \\ &\quad \times \sum_{d=0}^{t} \frac{t!}{d!} \Delta_1{}^d e^{-\left(\beta_{SR_o} - \delta_{SR_o}\right)\Delta_1}, \end{aligned} \tag{C.1}$$

and

$$\begin{aligned} I_6 &= 1 - \Pr\left\{\frac{P_{R_o}\left|h_{R_oD}\right|^2}{P_{J_n}\left|w_{R_{J_n}D}\right|^2 + \sigma_{R_oD}^2} < \Theta\right\} \\ &= 1 - \Pr\left\{\max_{i=1,2,\cdots,K} \frac{P_{R_i}\left|h_{R_iD}\right|^2}{P_{J_n}\left|w_{R_{J_n}D}\right|^2 + \sigma_{R_iD}^2} < \Theta\right\} \\ &= 1 - \prod_{k=1}^{K} \int_0^{\infty} f_{\left|w_{R_{J_n}D}\right|^2}(x) \int_0^{\frac{\Theta P_{J_n} x + \Theta \sigma_{R_iD}^2}{P_{R_i}}} f_{\left|h_{R_iD}\right|^2}(y)\, dy dx. \end{aligned} \tag{C.2}$$

Plugging (11) into (C.2), I_6 can be further calculated as

$$I_6 = 1 - \prod_{k=1}^{K} \left(1 - \frac{\varepsilon_{R_{J_n}D} P_{R_i}}{\varepsilon_{R_{J_n}D} P_{R_i} + \lambda_{R_iD} \Theta P_{J_n}} e^{-\frac{\lambda_{R_iD} \Theta \sigma_{R_iD}^2}{P_{R_i}}}\right). \tag{C.3}$$

Based on the (C.1) and (C.3), (53) can be derived.

(54) can be obtained when $a = 0$.

APPENDIX D PROOFS OF THEOREM 4, THEOREM 5 AND THEOREM 6

A. TRADITIONAL ROUND-ROBIN SELECTION

Substituting (60) into (59), we can obtain the following expression as

$$\begin{aligned} P_{int,TRRS}^{AN} &= 1 - \Pr\left\{\max\left\{C_{SE}, C_{R_iE}\right\} < C_{th}\right\} \\ &= 1 - \underbrace{\Pr\left\{C_{SE} < C_{th}\right\}}_{I_7} \underbrace{\Pr\left\{C_{R_iE} < C_{th}\right\}}_{I_8}, \end{aligned} \tag{D.1}$$

where

$$I_7 = F_{\left|\tilde{g}_{SE}\right|^2}(\Delta_4), \tag{D.2}$$

and

$$I_8 = 1 - \int_0^{\infty} f_{\left|w_{R_{J_n}E}\right|^2}(x) \int_{\frac{\Theta P_{J_n} x + \Theta \sigma_{R_iE}^2}{P_{R_i}}}^{\infty} f_{\left|h_{R_iE}\right|^2}(y)\, dy dx. \tag{D.3}$$

Similar to calculation of Appendix A, putting (9) and (11) into (D.3) and (D.1), (61) can be obtained.

(62) can be provided by setting $a = 0$.

B. SUBOPTIMAL RELAY SELECTION

Similar to Appendix D-1), substituting (64) into (59), the following expression can be obtained as

$$I_9 = \int_0^{\infty} f_{\left|w_{R_{J_n}E}\right|^2}(x) F_{\left|h_{R_cE}\right|^2}\left(\frac{\Theta P_{J_n} x + \Theta \sigma_{R_cE}^2}{P_{R_c}}\right) dx. \tag{D.4}$$

(65) can be derived by utilizing (D.2), (41) and (42).

When we set $a = 0$, (66) can be given.

C. OPTIMAL RELAY-RECEIVER PAIR SELECTION

Putting (68) into (59), we can obtain the relative expression as

$$\begin{aligned} I_{10} &= \Pr\left\{\max_{i=1,2,\cdots,K} \frac{P_{R_i}\left|h_{R_iE}\right|^2}{P_{J_n}\left|w_{R_{J_n}E}\right|^2 + \sigma_{R_iE}^2} < \Theta\right\} \\ &= \prod_{k=1}^{K} \int_0^{\infty} \varepsilon_{R_{J_n}E} e^{-\varepsilon_{R_{J_n}E} x} F_{\left|h_{R_iE}\right|^2}\left(\frac{\Theta P_{J_n} x + \Theta \sigma_{R_iE}^2}{P_{R_i}}\right) dx. \end{aligned} \tag{D.5}$$

According to Appendix D-1) and 2), we can obtain the (69).

(70) can be provided by setting $a = 0$.

REFERENCES

[1] A. Abdi, W. C. Lau, M. Alouini, and M. Kaveh, "A new simple model for land mobile satellite channels: First- and second-order statistics," *IEEE Trans. Wireless Commun.*, vol. 2, no. 3, pp. 519–528, May 2003.

[2] E. Lutz, D. Cygan, M. Dippold, F. Dolainsky, and W. Papke, "The land mobile satellite communication channel-recording, statistics, and channel model," *IEEE Trans. Veh. Technol.*, vol. 40, no. 2, pp. 375–386, May 1991.

[3] J. Liu, Y. Shi, L. Zhao, Y. Cao, W. Sun, and N. Kato, "Joint placement of controllers and gateways in SDN-enabled 5G-satellite integrated network," *IEEE J. Sel. Areas Commun.*, vol. 36, no. 2, pp. 221–232, Feb. 2018.

[4] Y. Shi, J. Liu, Z. M. Fadlullah, and N. Kato, "Cross-layer data delivery in Satellite-Aerial-Terrestrial communication," *IEEE Wireless Commun.*, vol. 25, no. 3, pp. 138–143, Jun. 2018.

[5] M. A. Vazquez, A. Perez-Neira, D. Christopoulos, S. Chatzinotas, B. Ottersten, P.-D. Arapoglou, A. Ginesi, and G. Tarocco, "Precoding in multibeam satellite communications: Present and future challenges," *IEEE Wireless Commun.*, vol. 23, no. 6, pp. 88–95, Dec. 2016.

[6] K. An, M. Lin, J. Ouyang, and W.-P. Zhu, "Secure transmission in cognitive satellite terrestrial networks," *IEEE J. Sel. Areas Commun.*, vol. 34, no. 11, pp. 3025–3037, Nov. 2016.

[7] L. Liang, S. Iyengar, H. Cruickshank, Z. Sun, C. Kulatunga, and G. Fairhurst, "Security for FLUTE over satellite networks," in *Proc. WRI Int. Conf. Commun. Mobile Comput.*, vol. 3, Jan. 2009, pp. 485–491.

[8] A. Kalantari, G. Zheng, Z. Gao, Z. Han, and B. Ottersten, "Secrecy analysis on network coding in bidirectional multibeam satellite communications," *IEEE Trans. Inf. Forensics Security*, vol. 10, no. 9, pp. 1862–1874, Sep. 2015.

[9] A. Roy-Chowdhury, J. S. Baras, M. Hadjitheodosiou, and S. Papademetriou, "Security issues in hybrid networks with a satellite component," *IEEE Wireless Commun.*, vol. 12, no. 6, pp. 50–61, Dec. 2005.

[10] N. Sklavos and X. Zhang, *Wireless Security and Cryptography: Specifications and Implementations*. Boca Raton, FL, USA: CRC Press, 2007.

[11] H. Cruickshank, M. P. Howarth, S. Iyengar, Z. Sun, and L. Claverotte, "Securing multicast in DVB-RCS satellite systems," *IEEE Wireless Commun.*, vol. 12, no. 5, pp. 38–45, Oct. 2005.

[12] A. D. Wyner, "The wire-tap channel," *Bell Syst. Tech. J.*, vol. 54, no. 8, pp. 1355–1387, Oct. 1975.

[13] N. Yang, S. Yan, J. Yuan, R. Malaney, R. Subramanian, and I. Land, "Artificial noise: Transmission optimization in multi-input single-output wiretap channels," *IEEE Trans. Commun.*, vol. 63, no. 5, pp. 1771–1783, May 2015.

[14] A. El Shafie, Z. Ding, and N. Al-Dhahir, "Hybrid spatio-temporal artificial noise design for secure MIMOME-OFDM systems," *IEEE Trans. Veh. Technol.*, vol. 66, no. 5, pp. 3871–3886, May 2017.

[15] R. Xu, X. Da, H. Hu, Y. Liang, and L. Ni, "Power and time slot allocation method for secured satellite transmission based on weighted fractional data carrying artificial noise," *IEEE Access*, vol. 6, pp. 65043–65054, 2018.

[16] C.-Y. Wu, P.-C. Lan, P.-C. Yeh, C.-H. Lee, and C.-M. Cheng, "Practical physical layer security schemes for MIMO-OFDM systems using precoding matrix indices," *IEEE J. Sel. Areas Commun.*, vol. 31, no. 9, pp. 1687–1700, Sep. 2013.

[17] F. Wu, C. Dong, L.-L. Yang, and W. Wang, "Secure wireless transmission based on precoding-aided spatial modulation," in *Proc. IEEE Global Commun. Conf. (GLOBECOM)*, Dec. 2015, pp. 1–6.

[18] J. Tang, H. Wen, L. Hu, H. Song, G. Zhang, F. Pan, and H. Liang, "Associating MIMO beamforming with security codes to achieve unconditional communication security," *IET Commun.*, vol. 10, no. 12, pp. 1522–1531, Aug. 2016.

[19] B. Evans, M. Werner, E. Lutz, M. Bousquet, G. E. Corazza, G. Maral, and R. Rumeau, "Integration of satellite and terrestrial systems in future multimedia communications," *IEEE Wireless Commun.*, vol. 12, no. 5, pp. 72–80, Oct. 2005.

[20] B. Paillassa, B. Escrig, R. Dhaou, M.-L. Boucheret, and C. Bes, "Improving satellite services with cooperative communications," *Int. J. Satell. Commun. Netw.*, vol. 29, no. 6, pp. 479–500, Nov. 2011.

[21] S. Sreng, B. Escrig, and M.-L. Boucheret, "Exact symbol error probability of hybrid/integrated satellite-terrestrial cooperative network," *IEEE Trans. Wireless Commun.*, vol. 12, no. 3, pp. 1310–1319, Mar. 2013.

[22] M. R. Bhatnagar and M. K. Arti, "Performance analysis of AF based hybrid satellite-terrestrial cooperative network over generalized fading channels," *IEEE Commun. Lett.*, vol. 17, no. 10, pp. 1912–1915, Oct. 2013.

[23] K. An, M. Lin, and T. Liang, "On the performance of multiuser hybrid satellite-terrestrial relay networks with opportunistic scheduling," *IEEE Commun. Lett.*, vol. 19, no. 10, pp. 1722–1725, Oct. 2015.

[24] K. An, M. Lin, J. Ouyang, Y. Huang, and G. Zheng, "Symbol error analysis of hybrid satellite–terrestrial cooperative networks with cochannel interference," *IEEE Commun. Lett.*, vol. 18, no. 11, pp. 1947–1950, Nov. 2014.

[25] A. Nosratinia, T. E. Hunter, and A. Hedayat, "Cooperative communication in wireless networks," *IEEE Commun. Mag.*, vol. 42, no. 10, pp. 74–80, Oct. 2004.

[26] M. Yuksel and E. Erkip, "Diversity in relaying protocols with amplify and forward," in *Proc. IEEE Global Telecommun. Conf. (GLOBECOM)*, vol. 4, Dec. 2003, pp. 2025–2029.

[27] P. K. Upadhyay and P. K. Sharma, "Max-max user-relay selection scheme in multiuser and multirelay hybrid satellite-terrestrial relay systems," *IEEE Commun. Lett.*, vol. 20, no. 2, pp. 268–271, Feb. 2016.

[28] W. Cao, Y. Zou, Z. Yang, and J. Zhu, "Relay selection for improving physical-layer security in hybrid satellite-terrestrial relay networks," *IEEE Access*, vol. 6, pp. 65275–65285, 2018.

[29] P. Lai, H. Bai, Y. Huang, Z. Chen, and T. Liu, "Performance evaluation of underlay cognitive hybrid satellite–terrestrial relay networks with relay selection scheme," *IET Commun.*, vol. 13, no. 16, pp. 2550–2557, Oct. 2019.

[30] K. Guo, K. An, B. Zhang, Y. Huang, D. Guo, G. Zheng, and S. Chatzinotas, "On the performance of the uplink satellite multiterrestrial relay networks with hardware impairments and interference," *IEEE Syst. J.*, vol. 13, no. 3, pp. 2297–2308, Sep. 2019.

[31] K. Guo, K. An, and X. Tang, "Secrecy performance for integrated satellite terrestrial relay systems with opportunistic scheduling," in *Proc. IEEE Int. Conf. Commun. Workshops (ICC Workshops)*, May 2019, pp. 1–6.

[32] J. Li, S. Han, X. Tai, C. Gao, and Q. Zhang, "Physical layer security enhancement for satellite communication among similar channels: Relay selection and power allocation," *IEEE Syst. J.*, vol. 14, no. 1, pp. 433–444, Mar. 2020.

[33] S. G. Izrail and M. R. Iosif, *Table of Integrals, Series, And Products*. New York, NY, USA: Academic, 2014.

[34] P. K. Sharma and D. I. Kim, "Secure 3D mobile UAV relaying for hybrid satellite-terrestrial networks," *IEEE Trans. Wireless Commun.*, vol. 19, no. 4, pp. 2770–2784, Apr. 2020.

[35] C. Loo, "A statistical model for a land mobile satellite link," *IEEE Trans. Veh. Technol.*, vol. 34, no. 3, pp. 122–127, Aug. 1985.

[36] K. Guo, K. An, B. Zhang, Y. Huang, and G. Zheng, "Outage analysis of cognitive hybrid satellite-terrestrial networks with hardware impairments and multi-primary users," *IEEE Wireless Commun. Lett.*, vol. 7, no. 5, pp. 816–819, Oct. 2018.

[37] K. Guo, M. Lin, B. Zhang, W.-P. Zhu, J.-B. Wang, and T. A. Tsiftsis, "On the performance of LMS communication with hardware impairments and interference," *IEEE Trans. Commun.*, vol. 67, no. 2, pp. 1490–1505, Feb. 2019.

[38] *Prediction Procedure for the Evaluation of Interference Between Stations on the Surface of the Earth at Frequencies Above About 0.1 GHz*, document ITU-R P.452-15, 2013.

[39] V. Bankey and P. K. Upadhyay, "Secrecy outage analysis of hybrid satellite-terrestrial relay networks with opportunistic relaying schemes," in *Proc. IEEE 85th Veh. Technol. Conf. (VTC Spring)*, Jun. 2017, pp. 1–5.

[40] J. N. Laneman, D. N. C. Tse, and G. W. Wornell, "Cooperative diversity in wireless networks: Efficient protocols and outage behavior," *IEEE Trans. Inf. Theory*, vol. 50, no. 12, pp. 3062–3080, Dec. 2004.

[41] T. Yoo and A. Goldsmith, "Capacity and power allocation for fading MIMO channels with channel estimation error," *IEEE Trans. Inf. Theory*, vol. 52, no. 5, pp. 2203–2214, May 2006.

[42] X. Li, M. Huang, C. Zhang, D. Deng, K. M. Rabie, Y. Ding, and J. Du, "Security and reliability performance analysis of cooperative multi-relay systems with nonlinear energy harvesters and hardware impairments," *IEEE Access*, vol. 7, pp. 102644–102661, 2019.

[43] J. Zhang, G. Pan, and Y. Xie, "Secrecy analysis of wireless-powered multi-antenna relaying system with nonlinear energy harvesters and imperfect CSI," *IEEE Trans. Green Commun. Netw.*, vol. 2, no. 2, pp. 460–470, Jun. 2018.

[44] K. Guo, K. An, Y. Huang, and B. Zhang, "Physical layer security of multiuser satellite communication systems with channel estimation error and multiple eavesdroppers," *IEEE Access*, vol. 7, pp. 96253–96262, 2019.

MENGYAN HUANG (Student Member, IEEE) received the B.S. degree in communication engineering (wireless mobile communication direction) from the Sias International College of Zhengzhou University, Zhengzhou, China, in 2017, and the M.Sc. degree in communication and information systems from Henan Polytechnic University, Jiaozuo, China, in 2020. She is currently studying in the State Key Laboratory of Integrated Services Networks (ISN), Xidian University, Xi'an China. Her current research interests include physical layer security, cooperative communication, and land mobile satellite communication.

FENGKUI GONG (Member, IEEE) was born in Shandong, China, in 1979. He received the M.S. and Ph.D. degrees from Xidian University, Xi'an, China, in 2004 and 2007, respectively. From 2011 to 2012, he was a Visiting Scholar with the Department of Electrical and Computer Engineering, McMaster University, Hamilton, ON, Canada. He is currently a Professor with the State Key Laboratory of Integrated Services Networks, Department of Communication Engineering, Xidian University. His research interests include cooperative communication, distributed space-time coding, digital video broadcasting systems, satellite communication, and 4G/5G techniques.

NAN ZHANG was born in Hubei, China, in 1980. She received the M.S. and Ph.D. degrees from Xidian University, Xi'an, China, in 2006 and 2012, respectively. Since then, she has been working with the School of Communication Engineering, Xidian University. Her research interests include cooperative communication, satellite communication, and channel coding.

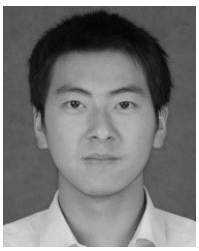

GUO LI (Member, IEEE) was born in Hanzhong, Shaanxi, China, in 1989. He received the B.S., M.S., and Ph.D. degrees in telecommunication engineering from Xidian University, Xi'an, in 2011, 2014, and 2017 respectively. From December 2015 to January 2017, he was a Visiting Ph.D. Student in electronic and computer engineering with McMaster University, Canada. Since 2018, he has been a Lecturer with the State Key Laboratory of Integrated Services Networks (ISN), Xidian University. His research interests include massive MIMO, cooperative relay transmission, space-time coding, array signal processing, and millimeter-wave communication.

FENG QIAN was born in Nantong, Jiangsu, China, in 1982. His current research interests include RF circuit and signal processing. He received the B.S. and M.S. degrees in communication engineering from Xidian University, Shaanxi, China, in 2007. From 2015, he was a Senior Engineer with the School of Communication and Information Engineering, Shanghai University, Shanghai, China.